



Page Proof Instructions and Queries

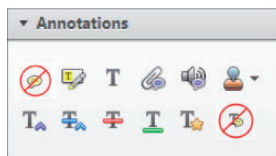
Journal Title: Journal of Rail and Rapid Transit, Proceedings of the Institution of Mechanical Engineers Part F [PIF]

Article Number: 596191

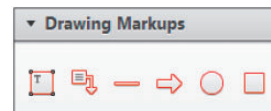
Greetings, and thank you for publishing with SAGE. We have prepared this page proof for your review. Please respond to each of the below queries by digitally marking this PDF using Adobe Reader.

Click "Comment" in the upper right corner of Adobe Reader to access the mark-up tools as follows:

For textual edits, please use the "Annotations" tools. Please refrain from using the two tools crossed out below, as data loss can occur when using these tools.











For formatting requests, questions, or other complicated changes, please insert a comment using "Drawing Markups."



Detailed annotation guidelines can be viewed at: <http://www.sagepub.com/repository/binaries/pdfs/AnnotationGuidelines.pdf>

Adobe Reader can be downloaded (free) at: <http://www.adobe.com/products/reader.html>.

No.	Query
	Please confirm that all author information, including names, affiliations, sequence, and contact details, is correct.
	Please review the entire document for typographical errors, mathematical errors, and any other necessary corrections; check headings, tables, and figures.
	Please confirm that the Funding and Conflict of Interest statements are accurate.
	Please ensure that you have obtained and enclosed all necessary permissions for the reproduction of artistic works, (e.g. illustrations, photographs, charts, maps, other visual material, etc.) not owned by yourself. Please refer to your publishing agreement for further information.
	Please note that this proof represents your final opportunity to review your article prior to publication, so please do send all of your changes now.
AQ: 1	Should this be reference 6, currently it is not cited in the 
AQ: 2	Can we add reference 18 here, currently it is not cited in the text 
AQ: 3	This paragraph was moved so that Figure 9(a) came before Figure 9(b) 
AQ: 4	Editor(s) conference location and dates, page numbers, publishers and publication location 
AQ: 5	Volume and page numbers 
AQ: 6	Editor(s), conference dates, page numbers, publishers and publication location
AQ: 7	Editor(s), page numbers, publishers and publication location 
AQ: 8	Editor(s), publishers and publication location 
AQ: 9	Figures 2,3,4,5,6(e),7,9,10,11 are poor quality images, please provide the better quality figure 

Windbreaks for railway lines: wind tunnel experimental tests



Gisella Tomasini, Stefano Giappino, Federico Cheli and Paolo Schito

Proc IMechE Part F:
J Rail and Rapid Transit
0(0) 1–13
© IMechE 2015
Reprints and permissions:
sagepub.co.uk/journalsPermissions.nav
DOI: 10.1177/0954409715596191
pif.sagepub.com



Abstract

A number of tests were carried out in the Politecnico di Milano wind tunnel to study the properties of different windbreak barriers for high-speed railway lines. A possible problem with the wind tunnel testing of these devices is the need to create wide scenarios (long barriers) and achieve high Reynolds number values in order to avoid scaling problems. In this study, two experimental campaigns were performed. In the first stage, the Reynolds number sensitivity was checked through specific tests in a high-speed test section ($Re_{max} = 7 \times 10^5$): it was found that, in the presence of barriers, the rolling moment coefficient is independent of the Reynolds number. A second experimental campaign was then carried out in a low-speed test section ($Re_{max} = 1.3 \times 10^5$) where a very long scenario was reproduced (150 m at real scale): barriers of different types, heights and porosities were tested. To compare them, forces and pressures on the vehicle model as well as forces on the barrier were measured.

Keywords

Windbreaks, crosswind, train, wind tunnel tests, force coefficients, pressure coefficients

Date received: 26 June 2014; accepted: 26 May 2015

Introduction

Crosswind effects on trains have, in the past decade, become one of the most widely studied problems in vehicle aerodynamics, due to their importance in railway safety. The development of new high-speed lines and rolling stock in Europe and Japan, the need for interoperability standards for trains travelling through the European Union¹ and the increasing importance of safety have focused the interest of researchers on the danger of train overturning induced by crosswinds.

Before the Technical Specification for Interoperability¹ in 2008, only a few European countries had National Standards focused on crosswind risk, and these standards were mainly based on experience rather than on real technical and scientific knowledge of the problem.^{2–5}

At present, the most common approaches used to reduce the risk of overturning induced by crosswinds include the following methods.

1. On the vehicle: aerodynamic optimization and reduction of the exposed lateral surface, in order to decrease the aerodynamic loads⁵ from the aerodynamic point of view, and actions on the weight, the mass distribution and the suspension characteristics, from the dynamic point of view.
2. On the infrastructure: both adoption of operational restrictions such as reduction of the

speed limit on bridges or viaducts^{7,8} and installation of windbreak barriers.⁹ Both of these solutions require a phase of preliminary study to locate high-risk areas.¹⁰ The second solution is preferred when the high-risk sites are short, as on viaducts or bridges.

The reduction of the maximum admissible vehicle speed as a function of the wind speed measured in proximity to the railway line is a procedure that has been adopted, in recent years on European high-speed lines such as the LN5 line in France (also known as the TGV-Méditerranée line⁷) and the Rome–Naples line in Italy.⁸ More recently, a specific task in the international project named ‘Aerodynamics in Open Air’ was devoted to the definition of risk analysis.

These methodologies are based on the calculation of characteristic wind curves^{1,11–13} that permit the evaluation of the maximum allowable vehicle speed for every section of a line and for every possible

Department of Mechanical Engineering, Politecnico di Milano, Italy

Corresponding author:

Gisella Tomasini, Department of Mechanical Engineering, Politecnico di Milano, via La Masa, 1, 20156 Milano, Italy.
Email: gisella.tomasini@polimi.it

wind velocity; over this speed limit, the overturning risk exceeds the safety limit.

Regarding windbreaks, an initial analysis of the sheltering effects of barriers with different features was carried out within the TRANSAERO project⁹ for high angles of attack with both still and moving models. Similar tests have also been performed in the Politecnico di Milano wind tunnel, on solid and porous barriers, using various scenarios.¹⁴ Barcala and Meseguer¹⁵ used wind tunnel tests to study the effects of a perpendicular wind on different parapets on bridges at a scale of 1:70. In recent years, some authors have approached the problem using computational fluid dynamics (CFD) studies in order to evaluate the effects of different fence parameters on trains, however the experimental validation of these simulations do not seem to have been adequately performed.^{15–17}

The work presented in this paper is part of a project funded by Rete Ferroviaria Italiana that was aimed at studying the effects of different windbreaks on train wind loads in order to design barriers for installation on Italian high-speed railway lines.

Wind tunnel tests on scale models often deal with competing requirements that cannot be completely satisfied. In this case, the request was to perform tests at a high Reynolds number to reduce scale model effects (Reynolds number in the order of a million) and also to create long infrastructure scenarios (with windbreak barriers) to avoid boundary effects being produced due to the short length of the barrier.

The Politecnico di Milano wind tunnel has two different test sections: the low-speed / boundary-layer test section (14×4 m, maximum wind velocity 16 m/s, turbulence intensity 1.5%) and the high-speed test section (4×4 m, maximum wind velocity 55 m/s, turbulence intensity 0.15%). The limited dimensions of the high-speed section make it impossible to obtain a complete analysis of the effects created by the barriers as a function of the angle of attack. However, the

larger dimensions of the boundary layer test section permit a long model-scale scenario, so that the effects of the barriers can be correctly reproduced for low angles of attack, but without having to investigate high Reynolds numbers. Based on the performance of the facilities, it was decided to split the tests into two stages. In the first stage, the Reynolds number sensitivity of the model was checked in the high-speed test section for high angles of attack (wind direction close to 90°). In the second stage, due to the larger dimensions of the low-speed test section, different windbreaks were tested on a 10-m long (model scale) infrastructure scenario scaled 1:15.

In both stages, tests were performed with a non-moving model of the ETR500 train set on single track ballast and rail (STBR) or double track ballast and rail (DTBR), and both the aerodynamic forces on the vehicle model and on a 1-m long barrier section were measured. In the conditions of a stationary train model, unlike real conditions, the wind speeds relative to the train and to the barriers are the same. This means that the forces measured at the barriers can be different than in reality. In any case, the purpose of this study was to compare a number of barriers by conducting a sensitivity study as a function of different parameters. Once the main effects of the barrier characteristics have been evaluated in terms of aerodynamic coefficients, a further development will be, in a future work, the simulation of relative motion between the train and the infrastructure through experiments or CFD simulations in order to study its effect on the force coefficients on both the train and the wind barrier.

Wind tunnel test setup

The ETR500 train was chosen as the reference vehicle for these tests. A 1:15-scale carbon fibre model was especially built in the Politecnico di Milano workshop (Figure 1). Based on the findings of previous experimental tests^{14,19}, it was expected that the most

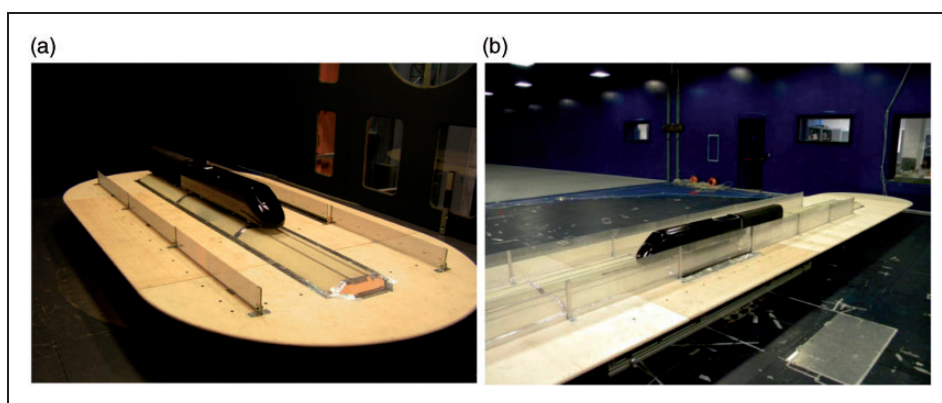


Figure 1. Wind tunnel tests on the ETR500 train: (a) on a STBR in the high-speed test section and (b) on a DTBR in the low-speed/ boundary-layer test section.

important aerodynamic forces would be experienced by the leading coach. Thus, the train model consisted of the locomotive and half of the trailing coach.

Scenario and windbreak types

Different scenarios were adopted in the two experimental campaigns (Figure 1): an STBR (the reference scenario for wind tunnel tests on trains²⁰) was used in the high-speed section (stage 1), whereas a DTBR was chosen for the low-speed room (stage 2), with the aim of reproducing a more realistic situation. Due to the dimensions of the test sections, in the high-speed section it was possible to reproduce a 3-m long model-scale infrastructure scenario (45-m full scale) whereas, in the boundary layer section, the reproduced track was 10-m long (150-m full scale). In both cases, the scenario was mounted on a splitter plate set at 0.3-m above the floor of the wind tunnel, to reproduce a block vertical velocity profile on the model.

The tested barriers can be classified in terms of their type, porosity and height (Table 1). Two specific types of barrier were considered:

- with uniform porosity, made of perforated steel sheets;

- horizontal band barriers, similar to the fences usually adopted on suspended bridges and made of aluminium bars.

Porosity is defined as the ratio of the open area to the total area of the barrier

$$\beta = \frac{A_{open}}{A_{total}} \quad (1)$$

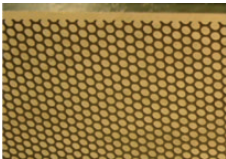

The heights of the tested barriers were measured from the splitter plate level and cover a range from 2 to 4 m (full-scale value). The position of the barrier in the two different scenarios is shown in Figure 2. In the second stage a real track layout is reproduced that has a DTBR with the barrier placed in its actual real-life position (Figure 2(b)).

Force measurements

During the wind tunnel tests, aerodynamic forces were measured on both vehicle and barrier models.

The locomotive model was mounted on an external six-component force balance located under the splitter plate (Figure 3(a)). To evaluate the wind force on the windbreaks, a 1-m long (model-scale) barrier section,

Table 1. Properties of the tested barriers: type, height (full-scale dimensions) and porosity (see equation (1)).

Barrier name	Type		Height h_B (m)	Porosity β (%)
B1H2	Perforated steel sheets		2	63
B1H4	Perforated steel sheets		4	63
B2H3	Perforated steel sheets		3	51
B2H4	Perforated steel sheets		4	51
B3H3	Perforated steel sheets		3	33
B3H4	Perforated steel sheets		4	33
B4H4	Horizontal bands		4	50

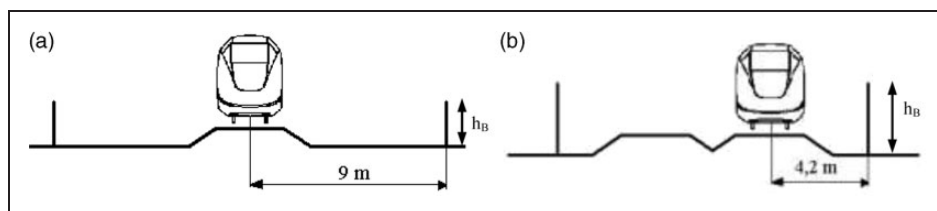


Figure 2. Wind tunnel tests on an ETR500 train: barrier position (full scale): (a) STBR scenario and (b) DTBR scenario.

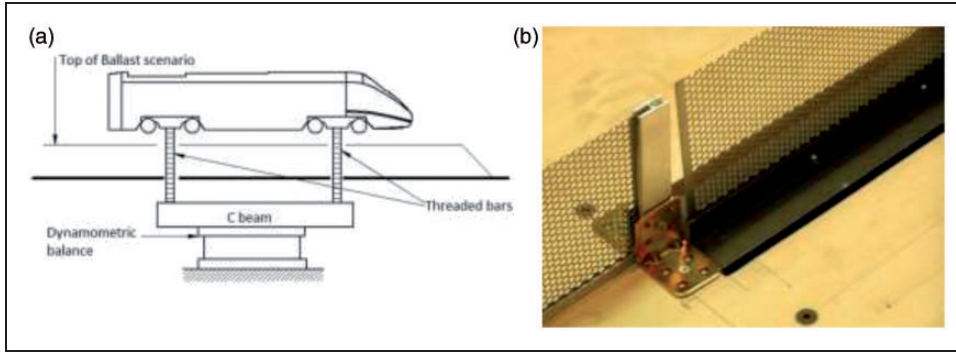


Figure 3. (a) The connection scheme between the dynamometric balance and vehicle model and (b) a photograph of the instrumented 1-m long barrier section.

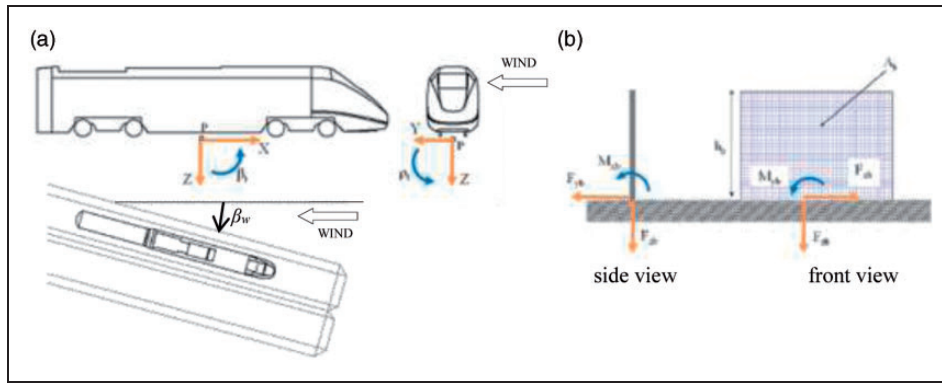


Figure 4. Reference frame system for force measurement on: (a) the vehicle and (b) the barrier section.

free of mechanical connections to the other barriers, was also mounted on a second external six-component force balance (Figure 3(b)). As shown in Figure 3, the vehicle was connected to the balance by means of two threaded bars set in correspondence with the bogies, whereas the barrier section was directly connected to the balance.

Forces (F_i) and moments (M_i) on the vehicle are expressed in a non-dimensional form as in the EN 14067-1 standard²¹

$$C_{Fi} = \frac{F_i}{\rho A U^2 / 2}, \quad C_{Mi} = \frac{M_i}{\rho A h U^2 / 2} \quad i = x, y, z \quad (2)$$

where ρ is the density of air, U is the mean input flow velocity and the characteristic dimensions of the cross-section A and length h are as in the standard²¹; their values were taken to be 10 m^2 and 3 m , respectively. The frame of the reference system (in agreement with the EN 14067-1 standard²¹) was fixed to the car body and its origin was located at the middle of the bogies, at track level (point P in Figure 4). Wind angles were considered to be positive when the train was located on the upwind rail. The rolling moment coefficient for the lee rail ($C_{Mx,lee}$) was also evaluated.²¹

The force/moment coefficients for the barrier were defined as

$$C_{Fib} = \frac{F_{ib}}{\rho A_b U^2 / 2}, \quad C_{Mib} = \frac{M_{ib}}{\rho A_b h_b U^2 / 2} \quad (3)$$

$$i = x, y, z$$

where h_b and A_b are the height of the barrier and the area of the instrumented section, respectively. The moment was reduced to the barrier base level (Figure 4).

Pressure measurements

For the tests carried out in the low-speed test section (stage 2), the vehicle model was also instrumented for pressure measurements: 158 pressure taps were positioned on the surface of the model, especially on the nose and on the connection surfaces between the side and upper part of the car body, where the highest pressure gradients occur. Figure 5 shows the layout of the pressure taps for some of the instrumented sections.

Surface pressure was measured using high-resolution multi-channel pressure scanners (PSI System 8400 with ESP-DTC pressure scanners, range $\pm 1 \text{ kPa}$, accuracy $\pm 0.10\%$ full-scale deflection

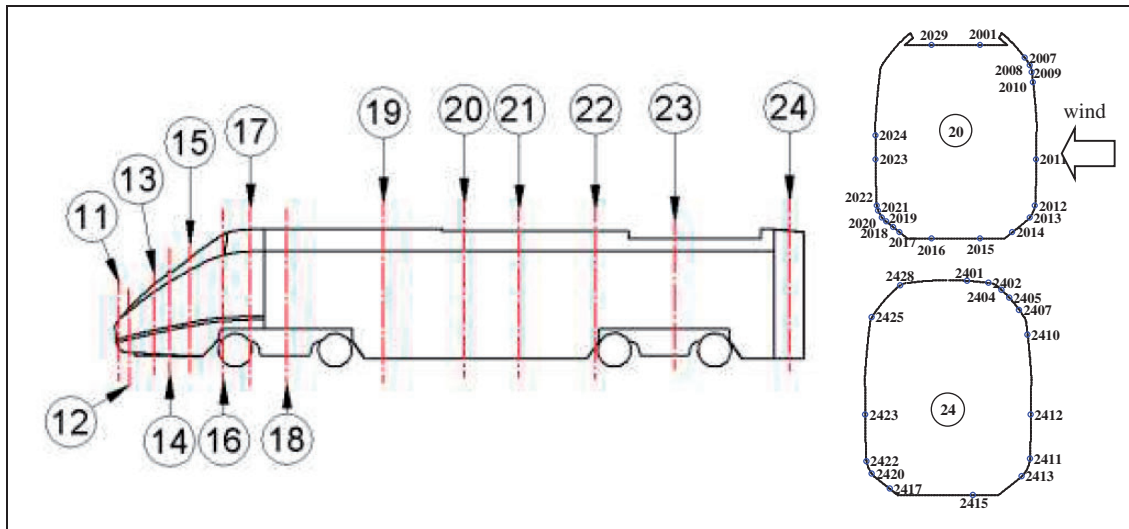


Figure 5. ETR500 train model: layout of the pressure taps in the considered sections.

(FSD)), hosted directly inside the model. Incoming wind speed was measured by a Pitot tube, connected to low-pressure micro-manometers (Furness FC0510, range 200–2000 Pa, accuracy 0.025% FSD).

Non-dimensional pressure coefficients were defined as follows

$$C_{Pi} = \frac{P_i - P}{\rho U / 2} \quad (4)$$

where P_i is the pressure at i th tap and P is the static pressure at the location of the model.

Stage I: Reynolds number sensitivity

The goal of the high-speed tests was to check if the Reynolds number had any effect on the vehicle's force coefficients, both with and without windbreak fences, and the barrier force coefficients. In these tests, Reynolds numbers ranging between 1.3×10^5 and 6.6×10^5 (based on a reference length of 3-m full scale) were investigated.

Vehicle force coefficients

The Reynolds number sensitivity of the vehicle model without barrier is investigated in detail in Cheli et al.²², thus, the main findings are summarized in Figure 6. Figure 6(a) and Figure 6(e) show, respectively, the lateral force and the rolling moment coefficient for the STBR scenario without barriers at different Reynolds numbers. It is possible to divide the diagrams into three sectors on the basis of the coefficient trend: an almost parabolic increasing trend, from 0° to about $\beta_w = 50^\circ$, a central sector with a negative slope, for angles of attack from 50° to 60° , and then a constant trend, up to 90° . In the first sector, the two coefficients are independent of the Reynolds number: in this range, the lateral force is

due to the wake width on the leeward side of the vehicle. At $\beta_w = 45\text{--}50^\circ$ (representing the critical angle for the considered vehicle), the coefficients reach their maximum value and then, above this angle, they decrease down to a constant value, showing a slight dependency on the Reynolds number and a large scatter in the data. This trend is due to the fact that, in the second sector, the flow behind the vehicle, in the leeward zone, is no longer driven by vehicle geometry; for this reason it is not able to produce large regions of negative pressure and, as a consequence, pressure recovery occurs.

These trends are typical of the crosswind problem and can be explained by considering changes in the aerodynamic behaviour of the first car from a slender body flow at low angles of attack, to bluff body behaviour with wind direction close to perpendicular. It is important to note that the effects due to the Reynolds number are negligible for low angles of attack, the most important ones in crosswind-related problems.

On the other hand, looking at Figure 6(c), the vertical force coefficient shows a Reynolds number dependency starting from low wind angles (about 25°) up to 90° .²²

Figure 6(b), Figure 6(d) and Figure 6(f) show the same vehicle aerodynamic coefficients but in this case measured for the presence of a B1H2 barrier: the tests with barriers were carried out for angles of attack higher than 30° , due to the point that, at lower angles, the finite length of the infrastructure model with barriers modifies the wind flow acting on the vehicle with respect to the real case, where the infrastructure has a pseudo-infinite length.

We observe that the effect of the Reynolds number almost disappears in this scenario. Also, the vertical force coefficient (Figure 6(d)) reveals a very low dependency on the Reynolds number. The reason for this behaviour is probably related to the properties

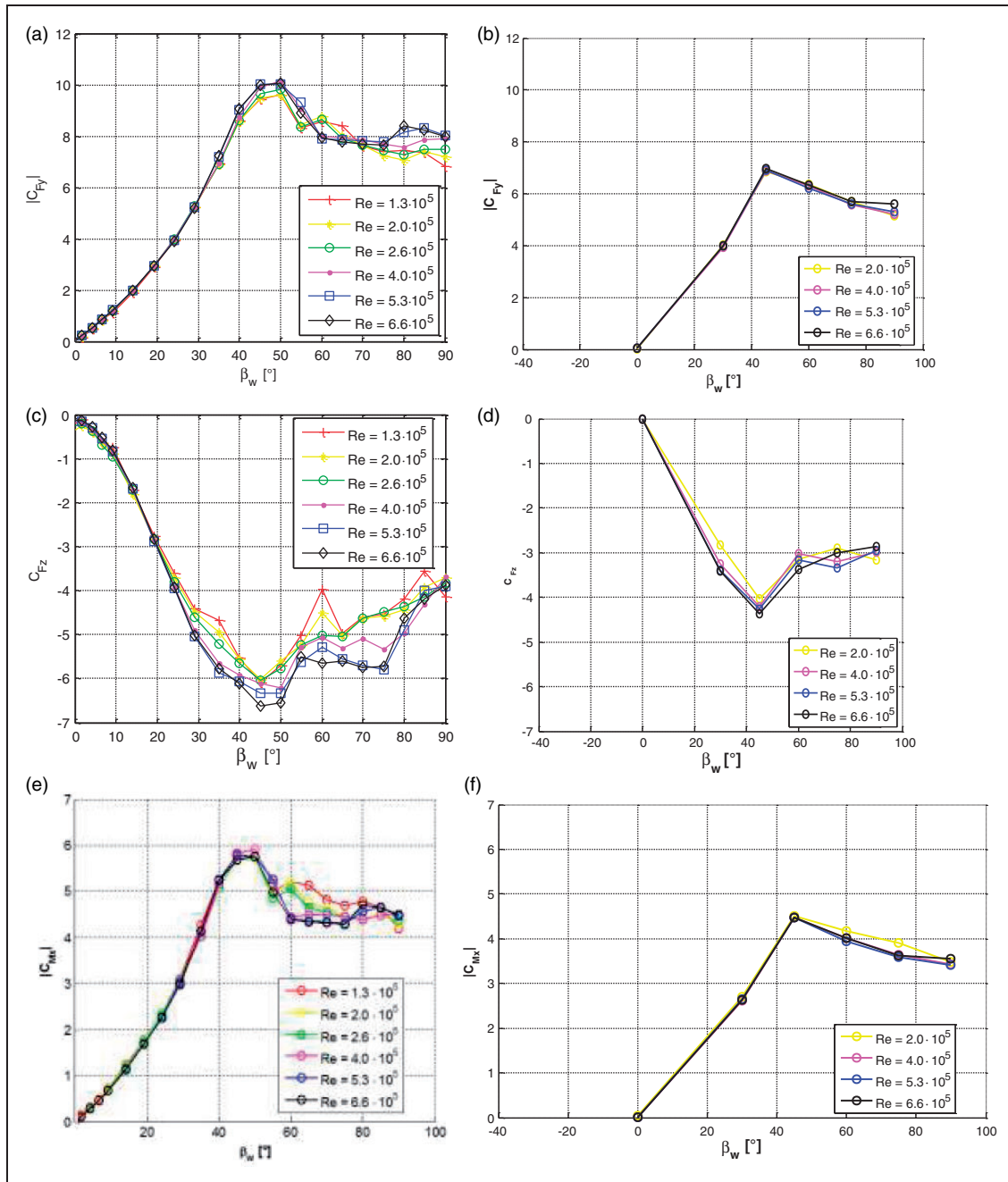


Figure 6. High-speed section, STBR: vehicle aerodynamic coefficients as a function of wind angle for different Reynolds numbers. With no barrier, on the left, and with a BIH2 barrier, on the right.

of the flow impacting on the train that is affected by the wake of the barrier. In fact, the wake has a higher turbulence level than the undisturbed flow and, in wind tunnel tests, Reynolds number effects are strongly related to flow turbulence characteristics, tending to decrease as the turbulence level increases.²²

Barrier force coefficients

The two coefficients of significance for barrier dimensioning are the normal force and rolling moment coefficients. Both these coefficients (Figure 7) show an increasing trend as a function of the wind angle. This behaviour is obviously due to the barrier surface

being exposed to the wind, which is at its maximum at 90°. The lateral force and the rolling moment coefficients show the same trend; this means that the height of the point of application of the lateral force remains unchanged as the wind angle varies. Finally, a dispersion of the coefficients as a function of the Reynolds number may be observed (about 12% of the variation of the rolling moment coefficient at 60°): the trend is not well-defined, however, and changes based on the wind angle range. On the basis of the available experimental data, neither coefficient seems to show a significant dependency on the Reynolds number.

The results of the high-speed test section tests, in terms of both vehicle and barrier coefficients, have

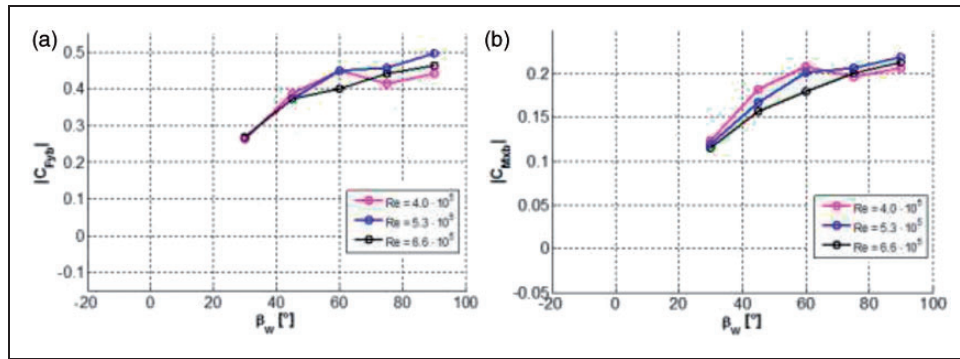


Figure 7. High-speed section, STBR, B1H2 barrier aerodynamic coefficients as a function of wind angle for different Reynolds numbers: (a) normal force coefficient and (b) rolling moment coefficient.

not demonstrated any significant dependency of the force/moment coefficients on the Reynolds number within the test wind velocity range investigated. This allowed us to perform a second test stage at low values of the Reynolds number, corresponding to the lower test speed in the stage 1 tests. These tests were conducted in the low-speed test section, where longer barrier scenarios could be reproduced.

Stage 2: Analysis of different windbreak types

The larger dimensions of the low-speed test section (14×4 m) allowed a wider scenario to be set-up so that the barrier effects could be investigated to low angles of attack. In a preliminary test, seven barriers were compared at a 90° wind angle, that is, with the wind perpendicular to the barrier and the train placed on the windward track. In a second test, two barriers, suitably selected from the seven previously tested, were investigated in depth by performing tests in the 0 – 90° wind angle range. In these tests the Reynolds number was equal to 1.3×10^5 (based on a reference length of 3-m full scale).

Preliminary tests at 90°

Figure 8 summarizes the results of the preliminary tests: the bars represent the train's rolling moment coefficient (scale on the left) for each barrier type, and these are sorted first by descending porosity and then by increasing height. Basically, we observe, as expected, that as the barrier porosity decreases and height increases, the train's rolling moment decreases. It is interesting to note that barrier B1H2 has no sheltering effect in the DTBR scenario, whereas it does have this effect in the STBR scenario, as shown in the previous section. This is because of the different distances between the train and the barrier in the two different setups; in fact, barrier position plays an important role in sheltering effects. This topic is not discussed here, but has been investigated with CFD simulations in Tomasini et al.²³

Comparing the performances of barriers B4H4 and B2H4, it can be observed that sheltering effects are quite different even though porosity and height are the same. The layout of the two barriers is in fact different (horizontal bands versus perforated sheets) and this has a major impact on sheltering properties.

In order to define the sheltering requirements for the windbreak barriers, numerical simulations were carried out using the characteristic wind curve approach.^{11,12} The train was required to be able to run at its maximum speed (300 km/h) in the presence of an unsheltered/upwind gust wind velocity of 50 m/s (worst-case scenario for the incoming direction). By setting this limit condition on the overturning risk and progressively reducing the train's aerodynamic forces, it was found that the desired barrier could reduce the rolling moment coefficient by about 30%; the dashed red horizontal line in the graph represents this value. Three barriers meet the requirements.

To select the best-performing barriers, the loads acting on the barriers themselves were analysed. The barrier's rolling moment coefficient is also reported in the graph, in green dots (scale on the right). As expected, when sheltering properties are increased, the load on the barrier itself grows. Since wind load is a key parameter in the design of a windbreak barrier, it should be kept as low as possible. For this reason, barrier B3H4, which had the highest barrier moment coefficient, was discarded at this stage.

Two barriers were then selected for in-depth investigation: B3H3 and B4H4. The first one has a lower porosity (33%) than the second one (50%) and is even lower in height (3 m compared with 4 m). The two selected barriers also differ in type: B3H3 has uniformly distributed porosity, whereas B4H4 is composed of equally distanced horizontal bars (see Table 1).

Complete tests on the selected windbreak fences

The train's vertical force and rolling moment coefficients in the presence of the selected barriers are shown in Figure 9; negative values of β_w indicate that the train is situated on the leeward track.

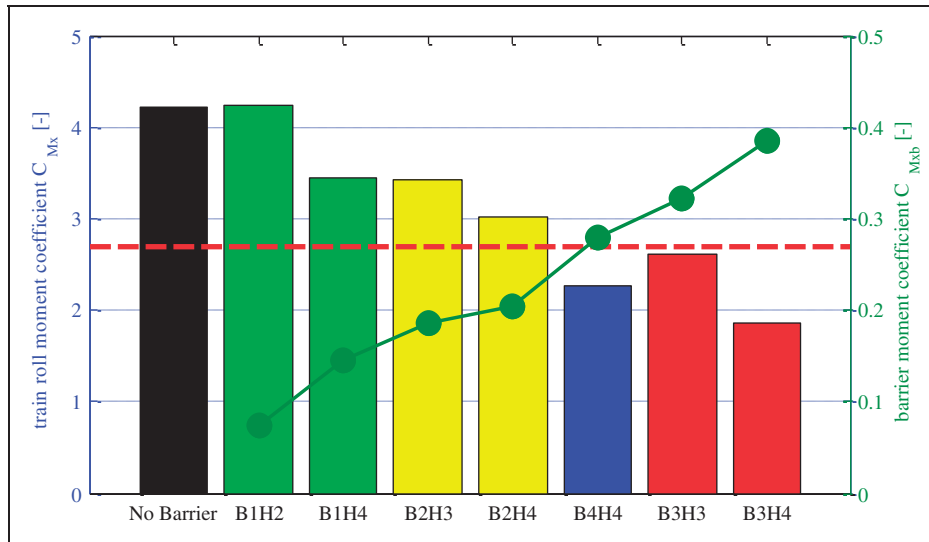


Figure 8. DTBR, wind angle 90° . Train's rolling moment coefficient for different barriers (bars, scale on the left) and corresponding barrier moment coefficients (green dots, scale on the right). The red horizontal line represents the threshold value set-up.

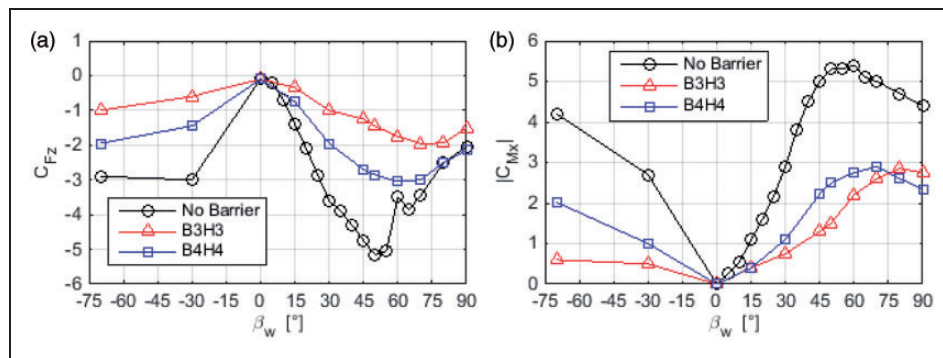


Figure 9. DTBR, comparison between train without barrier, with B3H3 and with B4H4: (a) train's vertical force coefficient C_{Fz} and (b) the train's roll moment coefficient C_{Mx} .

Looking at the vertical force coefficient (Figure 9(a)), it can be seen that both barriers create their best sheltering effect at low wind angles, less than 50° . At 90° this effect is actually zero for barrier B4H4 and very low for B3H3. As will be shown by analysis of the pressure coefficients, at high angles of attack, the barriers do not significantly modify the pressure distribution on the upper and lower part of the vehicle.

Looking at the rolling moment coefficient (Figure 9(b)), it can be observed that the two barriers have a significant effect on the reduction of loads on the train at all angles of attack, and that the maximum wind force is shifted toward higher angles of attack. The reduction of rolling moment due to both barriers with respect to the original value (without barrier) is higher than 30% for all wind angles.

Moreover, it can be seen that the trend in the moment coefficient is different in the two barriers: B3H3 is more effective at angles lower than 70° . This is because of the different designs of the two barriers: B3H3, made from perforated steel sheets

(uniform porosity), is more sensitive to wind exposure than the horizontal band one. A further investigation on the different effects of the two barriers on the train will be performed by analysing pressure distribution.

Finally, considering both coefficients, it may be noted that when the train is on the leeward track ($\beta_w, 0^\circ$, Figure 4), there is a further reduction in the force coefficients; in fact, as mentioned earlier, the distance between the train and the barrier plays an important role.²³ It can be confirmed that, for the barrier layout investigated, the most critical condition for the train overturning is when the train is running on the windward track.

Figure 10 shows pressure contour plots measured at a wind angle of 45° without barriers (Figure 10(a) windward and Figure 10(b) leeward), with barrier B4H4 (Figure 10(c) windward and Figure 10(d) leeward) and with barrier B3H3 (Figure 10(e) windward and Figure 10(f) leeward) whereas Figure 11 shows the same contour plot but for a yaw angle of 90° .

By observing Figure 10(c) and Figure 10(d) with respect to the situation without a barrier, it can be

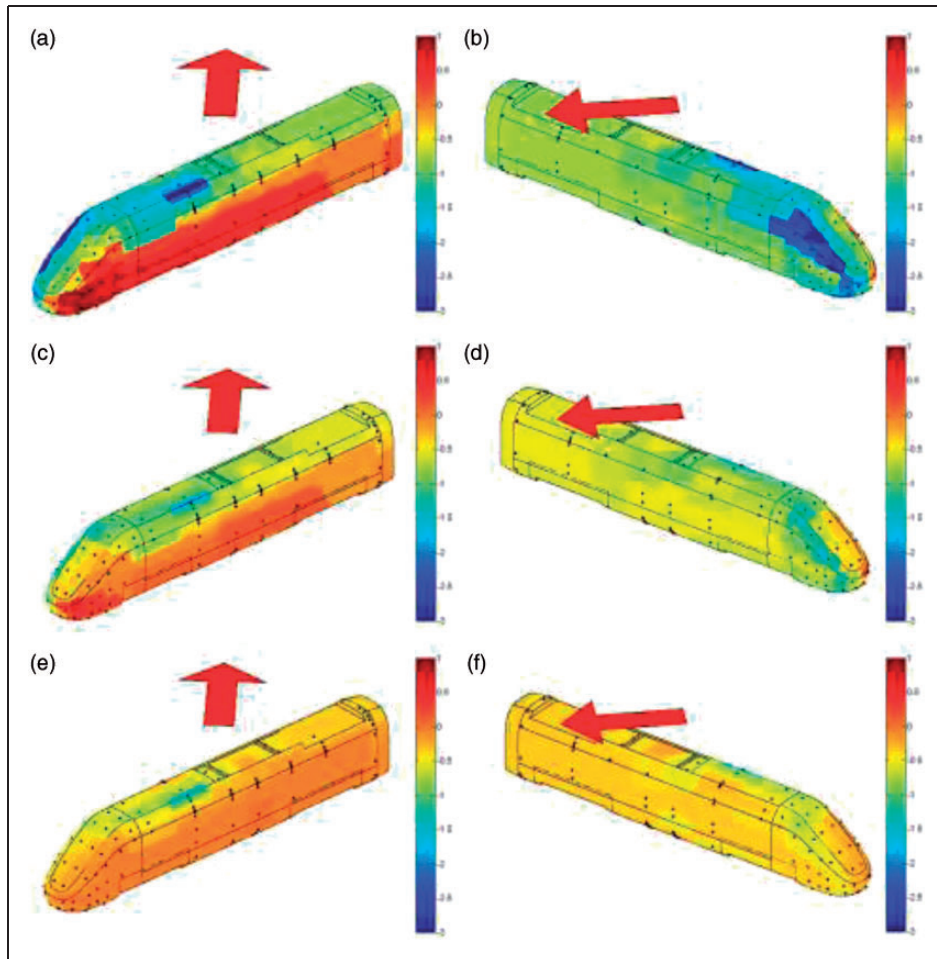


Figure 10. DTBR, pressure contour plot, wind angle $\beta_w = 45^\circ$: without barriers windward (a) and leeward (b), with B4H4 barriers windward (c) and leeward (d), with B3H3 barriers windward (e) and leeward (f).

seen that, as expected, barrier B4H4 reduces the pressure on the windward side, especially near the nose, but principally it reduces the negative pressure on the leeward side. This means that the barrier not only has an effect on the flow directly impacting the vehicle, but also it modifies the wake behind the train. The presence of barriers in front and behind the train generates a sort of channel that, especially at low wind angles, tends to drive the flow parallel to the train; the range of wind angles where the vehicle behaves as a slender body increases, and the maximum value is reached, as already observed, at higher angles of attack.

Looking at Figure 10(e) and Figure 10(f), the same effects found for barrier B4H4 can be seen, but they are more marked; barrier B3H3 significantly reduces the pressure on the windward side and negative pressure on the leeward side. The low and uniform porosity of this kind of barrier makes the pressure around the vehicle more uniform.

By analysing the effects of both barriers on the upper part of the vehicle, it is possible to understand why the vertical force coefficient at 45° is significantly lower with the barriers; the negative pressure in this

zone is greatly reduced all along the vehicle, especially with the B3H3 barrier.

At 90° the reduction of rolling moment coefficient due to the barriers is lower than at 45° , and that associated with the vertical force coefficient is almost zero.

Figure 11 shows that, unlike the case of a wind angle of 45° , the presence of the barriers mainly modifies the pressure distribution on the windward side of the vehicle. Only barrier B4H4 shows an additional small pressure recovery on the leeward side. In conclusion, at 90° the barriers reduce the flow pressure directly acting on the vehicle, however, they do not modify the behaviour of the flow behind the vehicle. In a similar way, the pressure on the upper part of the vehicle is not changed by the presence of barriers and, as a consequence, the vertical force coefficient with and without barriers remains unchanged.

To ensure a better understanding of the described phenomena, Figure 12 shows the pressure distribution measured with and without barriers on two vehicle sections at the same wind angles (the arrow pointing outwards represents negative pressure). Figure 12(a) and Figure 12(b) refer to $\beta_w = 45^\circ$; it can be seen that

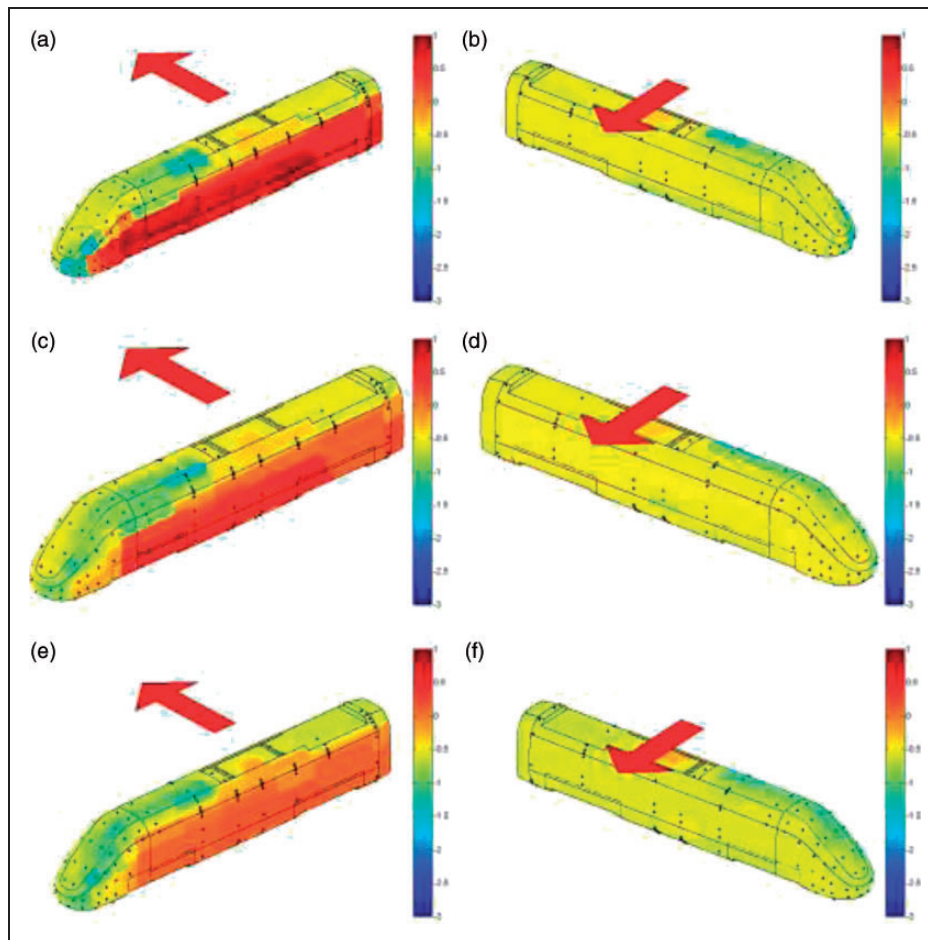


Figure 11. DTBR, pressure contour plot, wind angle $\beta_w = 90^\circ$: without barriers windward (a) and leeward (b), B4H4 barriers windward (c) and leeward (d), B3H3 barriers windward (e) and leeward (f).

the barriers produce a reduction in pressure all around the section, especially in the leeward zone and in the upper windward corner. There is also a reduction in negative pressure due to the barriers in the lower part of the vehicle; in any case, the combined effect on the upper and lower parts of the vehicle leads to a lower value for the vertical force.

Looking at the pressure distribution measured at 90° (Figure 12(c) and Figure 12(d)), the observations made for Figure 11 are evident. At this angle, the pressure distribution with and without the barriers is very similar; the main differences arise on the windward side, where the presence of the fences significantly reduces the positive pressure, and, occasionally, the under-body zone. In this area, the negative pressure associated with barrier B3H3 is larger than that measured without a barrier and with barrier B4H4; this behaviour justifies the reduction in the vertical force coefficient observed only for this windbreak (Figure 9).

Finally, Figure 13 shows the lateral force and rolling moment coefficients measured on the barrier; as previously observed, the two coefficients show the same trend and this means that the height of the point of application of the lateral force is constant.

Basically, the more the wind angle increases, rotating from parallel to the barrier (at 0°) to perpendicular to the barrier (at 90°), the higher the aerodynamic load on the barrier itself; in any case, as the wind angle increases, the slope of the curve decreases, and it is almost zero or negative at high wind angles. A comparison of the two barriers reveals that B3H3 is characterized by greater loads than B4H4 at all wind angles.

In conclusion, the perforated sheet barrier, although lower than the band barrier (3 m as compared with 4 m), given its lower and more uniform porosity, tends to better channel the flow along the vehicle at low wind angles, significantly reducing the negative pressure behind the train and, as a consequence, rolling moment. On the other hand, this barrier is subjected, at all wind angles, to a wind load about 20% higher than that of the B4H4 barrier, also around 90° , where this barrier performs less well. This implies higher costs in the dimensioning phase.

Conclusions

Extensive wind tunnel tests were carried out on different types of windbreak fences with a stationary train

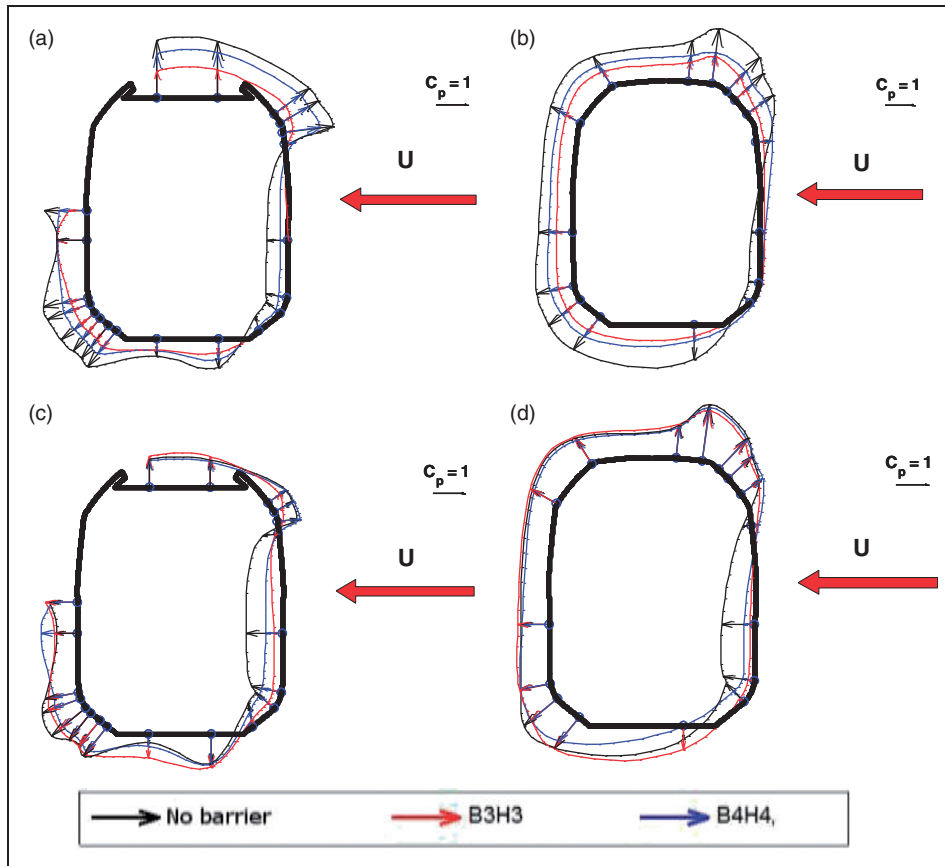


Figure 12. DTBR, pressure distribution plot: wind angle $\beta_w = 45^\circ$ for (a) section 20 and (b) section 24 (b); wind angle $\beta_w = 90^\circ$ for (c) section 20 and (d) and section 24.

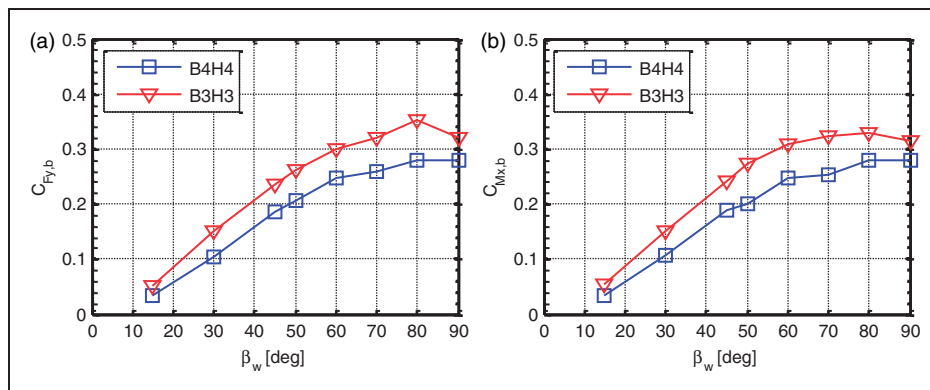


Figure 13. DTBR, comparison between B3H3 barrier and B4H4 barrier: (a) the barrier's lateral force coefficient $C_{Fy,b}$ and (b) the barrier's rolling moment coefficient $C_{Mx,b}$.

model. Force and moment coefficients were measured on both the vehicle model and a 1-m long barrier section; in addition, in order to understand the reasons for the differences in behaviour observed in terms of force coefficients, the pressures around the train model were also measured.

The first tests were carried out in the high-speed test section of the facility in order to evaluate the sensitivity of the force coefficients to the Reynolds number in the presence of barriers. It was shown that the installation of a barrier considerably

reduces the sensitivity of all train coefficients to the Reynolds number compared with the case without barriers. In particular, the dependency of the lateral force and rolling moment coefficients on the Reynolds number completely disappears, and that of the vertical force coefficient is significantly reduced.

This result allowed a second test campaign to be designed and carried out in the low-speed test section ($Re_{max} = 1.3 \times 10^5$) where longer barrier scenarios (150-m full scale) were built.

In this second campaign, preliminary tests were performed on seven barriers at $\beta_w=90^\circ$ to identify those most suitable for reducing overturning risk associated with crosswinds. Using as a target a reduction of the rolling moment coefficient of 30% and also considering the wind loads on barriers, two wind-break fences were selected for more detailed investigation: a perforated sheet barrier 3-m high with a porosity of $\beta=33\%$ (B3H3) and a horizontal band barrier (B4H4), higher (4m) but more porous ($\beta=50\%$).

It was shown that both barriers reduce the rolling moment coefficient by more than 30% at all wind angles. From the analysis of the pressure distribution, it was found that the presence of barriers not only reduces the pressure on the windward side, but also modifies the wake behind the train. At low wind angles, the barriers, especially the perforated sheet type, tend to drive the flow parallel to the train, reducing negative pressure behind the train and thus increasing the range in which the vehicle behaves as a slender body. Analysis of the barrier coefficients revealed that the perforated sheet barrier, which is less porous and performs better up to 70° , is subjected to a wind load 20% higher than that of the band barrier, at all wind angles.

Finally, it was observed that the distance between train and barrier is an important parameter in evaluating the barrier's performance and, in particular, the sheltering effect of barriers is higher when the train model is on the leeward track.

As already observed in the Introduction, one of the main limitations of these tests is that the relative motion between the train and the barrier is not reproduced in the test setup. In fact, using a stationary train model, it is possible to simulate the actual yaw angle (relative wind direction with respect to the train) but not the wind angle with respect to the barrier at the same time, having both the train and the barrier fixed. On the other hand, the results of these tests have yielded important information on the sheltering effects of wind barriers. In the future, it could be useful to reproduce the relative motion between train and infrastructure through experiments or CFD simulations to study its effect on the force coefficients on both the train and the wind barrier.

Starting from these experimental tests, a numerical CFD study was developed to analyse the sensitivity of barriers to a number of parameters.²³ The results of all these studies were used by Rete Ferroviaria Italiana for the design of new windbreaks on high-speed lines.

Acknowledgements

Rete Ferroviaria Italiana is acknowledged for its provision of the wind tunnel train models used in the tests. Finally, the authors wish to thank Dr M. Testa for his valuable contributions.

Funding

This research received financial support from Rete Ferroviaria Italiana.

References

1. TSI HS RST: 2008. Technical specification for interoperability of the trans-European high speed rail system.
2. Heine C, Möller M, Driller J and Tielkes T. A probabilistic approach to safeguard cross wind safety of passenger railway operation in Germany: the new DB guideline. In: *The eighth world congress on railway research*, South Korea, 2006.
3. Cléon LM, Gautier JP and Sourget F. Sécurité de la circulation des trains à grande vitesse vis-à-vis des vents latéraux: le programme DeuFraKo. *Rev Générale Chemins fer* 2006.
4. Imai T, Fujii T, Tanemoto K, et al. New train regulation method based on wind direction and velocity of natural wind against strong winds. *J Wind Engng Ind Aerodyn* 2002; 90: 1601–1610.
5. GM/RT2142: 2004. Resistance of railway vehicles to roll-over in gales.
6. Cheli F, Ripamonti F, Rocchi D and Tomasini G. Aerodynamic behaviour investigation of the new EMUV250 train to cross wind. *J Wind Engng Ind Aerodyn* 2010; 98: 189–201.
7. Cleon LM and Jourdain A. Protection of line LN5 against cross winds. In: *The fifth world congress on railway research*, Köln, Germany, 2006.
8. Cheli F, Diana G, Rocchi D, et al. A new stochastic approach for the regulation of the train velocity in presence of cross wind: an application on the Rome–Naples high-speed line. In: *The fifth international symposium on computational wind engineering*. Chapel Hill, NC, 23–27 May 2010.
9. Schulte-Werning B, Grégoire R, Malfatti A and Matschke G. *TRANSAERO - A European initiative on transient aerodynamics for railway system optimisation*. Berlin, Germany: Springer, 2002.
10. Freda A and Solari G. A pilot study of the wind speed along the Rome–Naples HS/HC railway line. Part 2-probabilistic analyses and methodology assessment. *J Wind Engng Ind Aerodyn* 2010; 98: 404–416.
11. Cheli F, Corradi R and Tomasini G. Crosswind action on rail vehicles: a methodology for the estimation of the characteristic wind curves. *J Wind Engng Ind Aerodyn* 2012; 104–106: 248–255.
12. Tomasini G and Cheli F. Admittance function to evaluate aerodynamic loads on vehicles: experimental data and numerical model. *J Fluids Struct* 2013; 38: 92–106.
13. Cheli F, Corradi R, Diana G and Tomasini G. A numerical-experimental approach to evaluate the aerodynamic effects on rail vehicle dynamics. *Veh Syst Dyn* 2004; 41: 707–716.
14. Boccione M, Cheli F, Corradi R, et al. Crosswind action on rail vehicles: wind tunnel experimental analyses. *J Wind Engng Ind Aerodyn* 2008; 96: 584–610.
15. Barcala MA and Meseguer J. An experimental study of the influence of parapets on the aerodynamic loads under cross wind on a two-dimensional model of a railway vehicle on a bridge. *Proc IMechE, Part F: J Rail Rapid Transit* 2007; 221(4): 487–494.

4

5

6

7

- 8
- 8
- 8
- 7
- 7
16. Li B, Xu Z, Yang Q and Feng S. Effects of railway wind fence on the aerodynamic forces of train and fence. In: *The 12th international symposium on structural engineering*, Wuhan, China, 17–19 November 2012, pp.625–630.
 17. Bi H, Ma G and Wang H. Aerodynamic characteristics of high-speed trains with wind fence. In: *The third international conference on transportation engineering*, Chengdu, China, 23–25 July 2011, pp.2521–2526.
 18. De Dios Sanz Bobi J, Suarez B, Núñez JG and Vázquez JAB. Protection high speed trains against lateral wind effects. In: *The ASME international mechanical engineering congress and exposition*, Lake Buena Vista, FL, 13–19 November 2009, pp.771–780.
 19. Cheli F, Corradi R, Rocchi D, et al. Wind tunnel tests on train scale models to investigate the effect of infrastructure scenario. *J Wind Engng Ind Aerodyn* 2010; 98(6–7): 353–362.
 20. EN 14067-6: 2010. Railway applications – aerodynamics – Part 6: requirements and test procedures for cross wind assessment.
 21. EN 14067-1: 2003. Railway applications - aerodynamics - Part 1: symbols and units.
 22. Cheli F, Rocchi D and Tomasini G. Study of the Reynolds effects on aerodynamic coefficients of a railway vehicle through wind tunnel tests. In: *The 13th international conference on wind engineering* Amsterdam, The Netherlands, 10–15 July 2011.
 23. Tomasini G, Cheli F, Schito P and Viganò A. CFD analysis on the effect of windbreaks on a train subjected to cross wind. In: *The fifth international symposium on computational wind engineering*, Chapel Hill, NC, 23–27 May 2010.